The effect of diameter of fibre on formation of hydrogen bonds and mechanical properties of 3D-printed PCL

Żaneta Górecka[a], Joanna Idaszek[a], Dorota Kołbuk[b], Emilia Choińska[a], Adrian Chlanda[a,c], Wojciech Święszkowski[a,*]

[a] Warsaw University of Technology, Faculty of Material Science and Engineering, Wołoska 141, 02-507 Warsaw, Poland
[b] Polish Academy of Sciences, Institute of Fundamental Technological Research, Pawińskiego 5b, 02-106 Warsaw, Poland
[c] Institute of Electronic Materials Technology, Department of Chemical Synthesis and Flake Graphene, Wólczyńska 133, 01-919 Warsaw, Poland

ABSTRACT

Fused Deposition Modelling (FDM) technique has been widely utilized in fabrication of 3D porous scaffolds for tissue engineering (TE) applications. Surprisingly, although there are many publications devoted to the architectural features of the 3D scaffolds fabricated by the FDM, none of them give us evident information about the impact of the diameter of the fibres on material properties. Therefore, the aim of this study was to investigate, for the first time, the effect of the diameter of 3D-printed PCL fibres on variations in their microstructure and resulting mechanical behaviour. The fibres made of poly(ε-caprolactone) (PCL) were extruded through commonly used types of nozzles (inner diameter ranging from 0.18 mm to 1.07 mm) by means of FDM technique. Static tensile test and atomic force microscopy working in force spectroscopy mode revealed strong decrease in the Young's modulus and yield strength with increasing fibre diameter in the investigated range. To explain this phenomenon, we conducted differential scanning calorimetry, wide-angle X-ray-scattering, Fourier-transform infrared spectroscopy, infrared and polarized light microscopy imaging. The obtained results clearly showed that the most prominent effect on the obtained microstructures and mechanical properties had different cooling and shear rates during fabrication process causing changes in supramolecular interactions of PCL. The observed fibre size-dependent formation of hydrogen bonds affected the crystalline structure and its stability. Summarising, this study clearly demonstrates that the diameter of 3D-printed fibres has a strong effect on obtained microstructure and mechanical properties, therefore should be taken into consideration during design of the 3D TE scaffolds.

1. Introduction

Tissue engineering (TE) combines life sciences, chemistry and engineering to develop treatment strategies of damaged tissues and organs. In one of the TE approaches, 3D artificial matrices (scaffolds) are used. To enable cell adhesion and organization, the scaffolds should be made of biocompatible materials and possess open porosity, among others. Moreover, the shape and size of the pores should be carefully designed as it determines stiffness and permeability of the scaffold and, therefore, its biological performance [1].

Fused Deposition Modelling (FDM) [2–5] and its modifications, i.e. 3D Fibre Deposition [5–11], 3D Plotting [12–16] and Precision Extruding Deposition [5,17,18] are examples of additive manufacturing techniques. They are based on deposition of melt of polymer in a form of fibres in a layer-by-layer fashion. All aforementioned techniques are widely used in TE to fabricate 3D porous scaffolds as they are computer-aided, thus ensure high shape fidelity and reproducibility [2–18].

By varying the distance between individual fibres and deposition angle in consecutive layers of a scaffold, size and shape of pores can be adjusted. This in turn yields different porosity and mechanical properties and has significant impact on biological performance of the scaffolds [2,19–21].

Mechanical properties of scaffolds depend not only on the architecture thereof but also on bulk properties of used material. Those, in turn, are determined by polymer chemistry, molecular weight (MW), degree of crystallinity and macromolecular arrangement. For example, poly(L-lactide) has stiffness superior to that of poly(ε-caprolactone), PCL [22,23]. Regarding the MW, low-MW PCL (M_w ~14 kDa) has stiffness lower than high-MW PCL (M_w ~65 kDa) [24]. However, further increase in MW leads to decrease in crystallinity, and thus stiffness of the polymer bulk [25,26]. Additionally, mechanical properties might be tailored by manipulating the crystallinity and molecular orientation.

The former can be enhanced by post-extrusion annealing at increased temperatures or drawing during fibres formation [27–30]. The latter may be affected by increase of shear stress during processing of semi-crystalline polymers causing changes in microstructure and mechanical properties [31,32]. In the case of extrusion of polymer melt, the molecular order increases with shear stress which can be modulated, e.g. by diameter of the nozzle [31].

All the aforementioned reports suggest that mechanical properties of the building blocks of an FDM-scaffold, i.e. the deposited fibres, might depend on diameter thereof. However, this parameter was not comprehensively investigated from microstructural point of view. In the majority of the reported studies utilizing the FDM in TE, the fibre diameter was set to be a constant value while other parameters (e.g. fibre spacing, deposition angle or shift of fibres in n + 2 layer) were altered [1,19,33]. In the few studies, where the fibre diameter was changed during scaffold fabrication, the possible variations in obtained microstructures were omitted. Moreover, the mechanical properties of the designed constructs were evaluated in the context of porosity and not fibre diameter [2,10]. However, the systematic study explaining phenomena governing a manifold-scaled changes in microstructure occurring during FDM fabrication of PCL fibres is still missing.

The aim of this study was to investigate for the first time the effect of diameter of 3D-printed PCL fibres on their microstructure and mechanical properties. To this end, PCL-fibres were extruded through nozzles with various inner diameters ranging from 0.18 mm to 1.07 mm using the FDM printer. Static tensile testing and atomic force microscopy (AFM) were used to evaluate mechanical properties of the fibres in the macro and nanoscale. In order to reveal the underlying causes of the observed relation between the diameter and the mechanical performance the differences in microstructure of extruded fibres were investigated by differential scanning calorimetry (DSC), wide-angle X-ray scattering (WAXS), Fourier-transform infrared spectroscopy (FTIR) and polarized light microscopy (PLM). Moreover, the infrared (IR) imaging was performed to study the change of temperature of PCL fibres during printing.

2. Materials and methods

Poly (ε-caprolactone) (PCL, Mn 70,000–90,000, granules, Aldrich, UK) and methylene chloride (Chempur, Poland) were used to prepare polymeric films by solvent casting method. After dissolution of the granules, the solution was cast into glass Petri dishes and dried overnight under the hood at room temperature. Obtained films were additionally dried for 72 h in vacuum dryer (35 °C, $p = 100$ mbar) and stored at 25 °C (p = 100 mbar).

2.1. Fabrication of fibres

Fibres were fabricated by Precision Extruding Deposition (a modified FDM method), using BioScaffolder (SYSENG, Germany). Material was heated to 100 °C and extruded through six different nozzles (EZ-FLO Encapsulation Needle, DL Technology, USA) with inner diameters (ID) ranging from 0.18 mm to 1.07 mm. To fabricate single fibres with circular cross section, the PCL melt was deposited on a house-made platform (Fig. 1) designed to ensure reduced contact with the platform and thus limiting deformation of the fibres. The fibres were deposited at the distance of 2.5 ID. The parameters of the printing (XY feed rate and spindle screw speed) were adjusted to obtain regular 40 mm long fibres with the diameter corresponding to inner diameter of the used nozzles. To calculate apparent shear rate ($\dot{\gamma}$) at the walls of the nozzles, we used Eq. (1) which was applied by Pezzin and co-workers in capillary extrusion experiments [34]:

$$\dot{\gamma} = \frac{32Q}{\pi D^3} \tag{1}$$

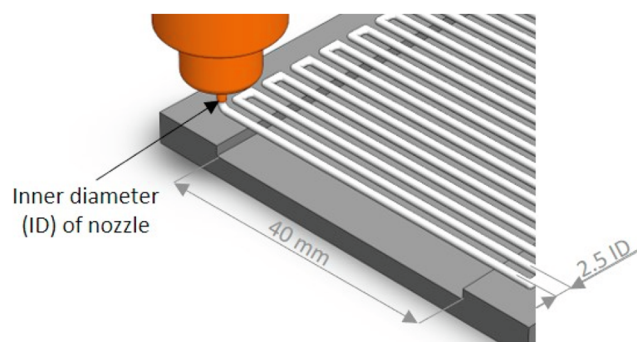where Q is a flow rate determined experimentally, and ID is the inner

Fig. 1. The visualisation of platform for fabrication of fibres with 1.07 mm fibres printed on it.

diameter of a nozzle. The fibres after fabrication were stored at room temperature for 1 month before further experiments to ensure the relaxation of microstructure.

2.2. Infrared (IR) imaging

IR imaging was performed during extrusion process with thermographic camera V50 (VIGO System S.A., Poland) equipped with standard lenses. The field of view of camera covered a fixed area of printing platform. Thermograms were taken automatically every 5 s. From single thermogram, the linear profile of temperature was analysed. Observation was carried out for 3 types of nozzles with ID 1.07 mm, 0.41 mm and 0.25 mm.

2.3. Tensile testing

In order to determine the Young's Modulus (E) of fibres with various diameters, static tensile testing was carried out on a MicroTester 5943 (Instron, USA) with rate equal 1%/min of the initial length ($L_0 = 10$ mm). E was calculated according to ISO-527 norm using linear regression in the range from $\varepsilon_1 = 0{,}0005$ to $\varepsilon_2 = 0{,}0025$ of the stress-strain curve. From the same test, yield strength (σ_1) was determined by the offset method at strain of 1% of the initial length. Five fibres of each type were tested in the strain range up to necking.

2.4. Atomic force microscopy (AFM)

Apparent Young's modulus (E_{JKR}) values were estimated using Force Spectroscopy AFM mode. The measurement is based on the acquisition of so-called force-distance curves that correspond to relation between the deflection of a scanning probe and relative position of microscope's piezoelectric scanner. Probe deflection suits to the force between the end of the scanning probe and the surface of the tested sample.

The cross sections of fibres were prepared using ultramicrotome (EM UC7, Leica) equipped with a glass knife at −70 °C. Two different areas were measured in the centre of each sample and > 1000 curves were acquired over every tested area of $10 \times 10\,\mu m$. In our research, E_{JKR} value was determined according to the principles of JKR (Johnson-Kendall-Roberts) [35,36] model according to Eq. (2):

$$E_{JKR} = \frac{3P_{JKR}}{4\sqrt{R}\left(h^{\frac{3}{2}}\right)} \tag{2}$$

where: R is the scanning probe's curvature, h is the indentation depth and P_{JKR} is the reduced pressure force.

Prior to the experiment, the scanning probes (RC800PSA-no.3 from Olympus, Japan) were calibrated using Thermal Tune method. Scanning probe with 15 nm radius was chosen, since smaller radius of the probe may cause overestimation of Young's modulus value [37]. AFM measurements were done under ambient conditions in air, at

Table 1
Parameters of fabrication of fibres: ID – inner diameter of nozzle, T – temperature, p – pressure, F – XY feed rate, VD – Spindle screw speed, Q – flow rate, $\dot{\gamma}$ – shear rate, OD – obtained diameter (± SD).

ID [mm]	T [°C]	p [MPa]	F [mm/min]	VD [rpm]	Q [ml/h]	$\dot{\gamma}$ [1/s]	OD [mm]	
0.18	100	0.5	20	180	0.20	96.3	0.182	± 0.005
0.25			70	180	0.40	72.2	0.242	± 0.003
0.33			95	200	0.95	75.1	0.326	± 0.008
0.41			85	200	1.34	54.9	0.428	± 0.008
0.58			40	180	2.38	34.5	0.608	± 0.020
1.07			55	100	3.11	7.2	1.022	± 0.027

25 ± 2 °C and humidity 30 ± 2% on MFP3D-BIO AFM from Asylum Research/Oxford Instruments equipped with extended (40 μm) Z scanner. Data processing was conducted with Igor Pro (ver. 6.37) software provided by the microscope producer.

2.5. Differential scanning calorimetry (DSC)

DSC was used to determine the thermal properties and the degree of crystallinity of the fibres. Measurements were carried out using Q2000 apparatus (TA Instruments). The samples were cooled to −80 °C and then heated to 120 °C with heating and cooling ramp of 10 °C/min. The degree of crystallinity X_c was calculated according to Eq. (3) from the first heating cycle:

$$X_c = 100\% \cdot \Delta H_m / \Delta H_f^0 \tag{3}$$

where: ΔH_m – enthalpy of fusion of sample [J/g], ΔH_f^0 – enthalpy of fusion of 100% crystalline PCL (142 J/g) [J/g] [38].

2.6. Wide-angle X-ray scattering (WAXS)

WAXS technique was applied for analysis of crystallinity and nanostructure of the PCL fibres. WAXS measurements were performed using Bruker D8 Discover diffractometer operated at the voltage of 40 kV, current of 20 mA and CuKα radiation with wavelength of 0.1542 nm. All measurements were performed in reflection mode. The angular range of measurements, 2Θ, was between 5° and 35°. Considering overlapping of diffraction peaks from crystal peaks of PCL, peaks on WAXS radial profiles from crystal and amorphous phases were deconvoluted using Pearson VII and Gauss function, respectively [39]. From this data, degree of crystallinity, position of peak from main crystal lattices (110), (111) and (200) and crystallite sizes were determined.

The crystallite size L was calculated by Scherrer Eq. (4) [40]:

$$L = \frac{K\lambda}{\beta cos\theta} \tag{4}$$

where L is the crystallite dimension, or coherence length, perpendicular to the $(hk\ell)$ plane, K (= 0.9) is the Scherrer constant, β is line broadening at half the maximum intensity, λ is the wavelength of the X-rays and θ is the Bragg angle.

2.7. Fourier-transform infrared spectroscopy (FTIR)

The infrared spectra were recorded using Nicolet 8700 FTIR spectrometer. Measurements in ATR mode with diamond crystal were made with resolution of 4 cm^{-1} and 128 scans. Data were collected and analysed in the dedicated Omnic software. In order to determine the ratio of crystalline and amorphous phase, the PCL carbonyl band (1600-1820 cm^{-1}) was deconvoluted [41–43]. The obtained PCL carbonyl band peak was automatically resolved into four components Voight's peaks. The main peaks derived from amorphous band (peak "4") and a crystalline band (peak "3") had maxima fixed at 1732 cm^{-1} and in the range 1720–1722 cm^{-1}, respectively. Other two peaks, called peaks "1" and "2", were fixed at 1690 cm^{-1} and 1700 cm^{-1} and their FWHM was

set as 25 cm^{-1}. Performed procedure enabled detailed analysis of changes in area and the position of the main peaks. The degree of crystallinity X_c was calculated as a ratio of Ac/(Ac + Aa), where Aa was the area of peak "4" derived from amorphous band (A4) and Ac was estimated in two ways; as the area of crystalline band (A3, from peak "3") with or without areas of additional peaks "1" (A1) and "2" (A2) (which originate from interactions of carbonyl groups in the C=O···CH$_2$ hydrogen bonding) [43,44].

2.8. Polarized light microscopy (PLM)

The polarizing-interference microscope MPI 5 (PZO Co, Poland) was used for the analysis of size of spherulites. Investigated samples were in a form of 1 μm-thick slices obtained during cryo-sectioning (−70 °C) using ultramicrotome (EM UC7, Leica) equipped with a glass knife. Before cutting, fibres were embedded in a chloroprene rubber-based glue (Klej guma-metal, Dragon, Poland) which easily enabled to obtain ultra-thin slices. Foils were collected on standard glass slides and covered with coverslips.

3. Results

Fibres with diameters in the range of 0.18 mm to 1.07 mm were fabricated by FDM using six different nozzles. To obtain smooth surface and desired diameter of fibres, feed rate was adjusted experimentally between 20 and 95 mm/min with the maximum for nozzle ID 0.33 mm (Table 1). First, the profiles of temperature in longitudinal direction were recorded to visualise the difference in cooling rates between fibres. In the next steps, the mechanical properties of fibres and various analyses of the degree of crystallinity and microstructure were conducted.

3.1. Temperature of surface during fabrication process

Temperature profile of the surface along the longitudinal direction of the extruded 0.25 mm, 0.41 mm and 1.07 mm fibres of PCL was measured from the collected thermograms (Fig. 2a). Difference in the recorded initial temperature of the extruded fibres were observed (Fig. 2b); it was 54 °C, 44 °C and 36 °C for1.07 mm, 0.41 mm and 0.25 mm fibres, respectively. Moreover, the IR imaging showed various slopes of cooling profiles recorded during extrusion of the investigated fibres, with cooling rate of 1.07 mm fibres being much lower than of the other two. After 30 s of spontaneous cooling, the temperature of the 1.07 mm fibres reached approx. 26 °C and remained constant for approx. another 30 s. Afterwards, the 1.07 mm fibres equilibrated to the ambient temperature (22 °C). Here, it should be emphasized that the obtained results are used just for illustration of the phenomenon, and they should not be considered as quantitative data due to the resolution of the camera.

3.2. Mechanical properties

Fabricated PCL fibres were submitted to a static tensile test. The obtained results showed strong converse correlation between the
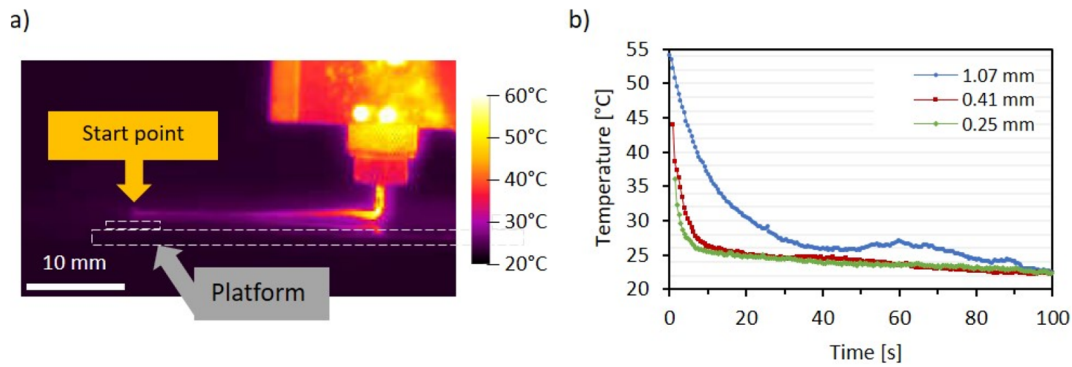
Fig. 2. The results obtained during IR observations: a) the thermogram after 1 min of printing of fibres thru nozzle with ID 1.07 mm (the ambient temperature was 22 °C) and b) the change of temperature of 1.07 mm, 0.41 mm and 0.25 mm fibres after extrusion.
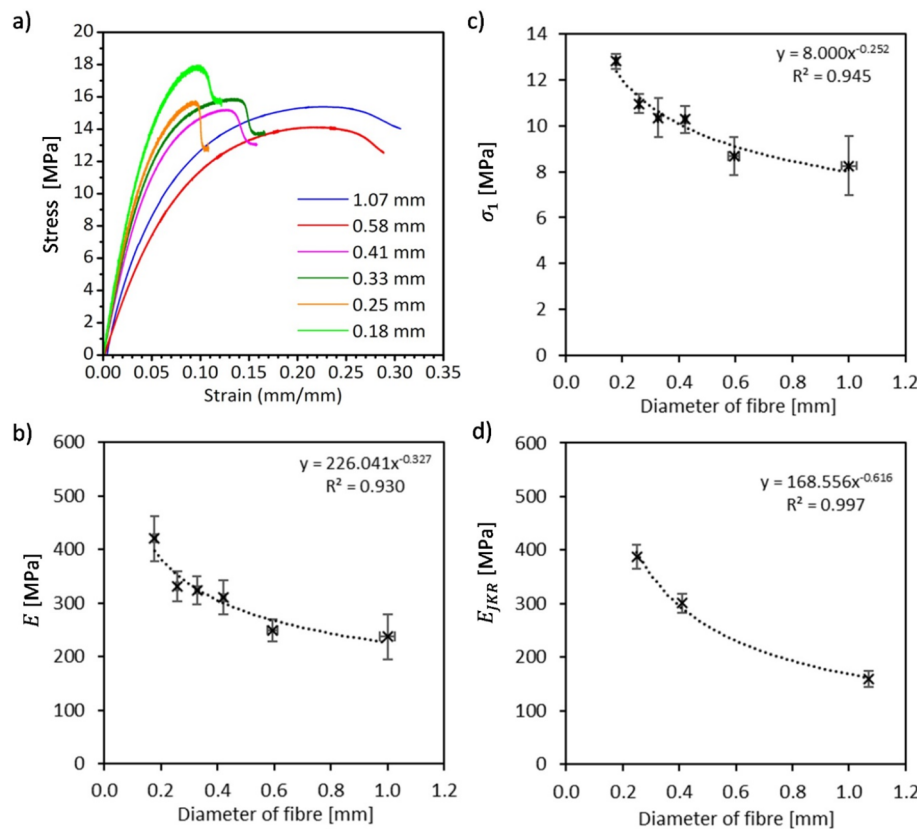

Fig. 3. a) The engineering stress-strain curves of representative samples in tensile test; b) Young's modulus and c) yield strength as a function of fibre diameter measured by static tensile test; d) apparent Young's modulus E_{JKR} estimated for fibres 0.25 mm, 0.41 mm and 1.07 mm using AFM working in force spectroscopy mode.
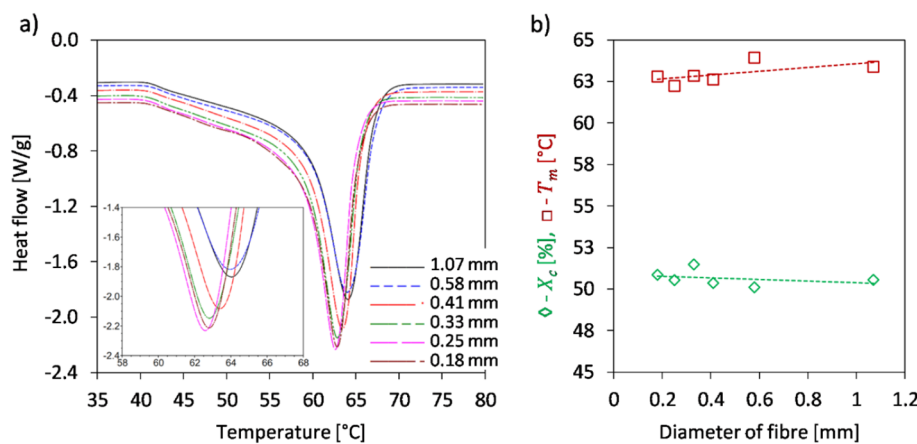

Fig. 4. a) The heat flow during melting as a function of fibre diameter recorded during DSC measurements. The offset between signals is applied to ensure easier analysis. The presented endotherms are from first heating run. The insert shows the position of peaks minima, b) the relation between fibre diameter and melting temperature (□) and crystallinity (◊) based on the heat of fusion of the fabricated fibres. The results were obtained from first heating run.

diameter of the extruded fibres and measured mechanical properties (Fig. 3b and c). The thicker fibres exhibited both lower values of E and lower yield strength. The post hoc one-way ANOVA with a Tukey–Kramer pair-wise comparison test of the results showed significant differences between majority of pairs for all compared subgroups (Table A1 in Supplementary Data). The difference between the marginal values of E was approx. 44%: 420 ± 42 MPa for 0.18 mm and 237 ± 42 MPa for 1.07 mm. For σ_1, it was 12.8 ± 0.5 MPa and 8.3 ± 1.3 MPa for 0.18 mm and 1.07 mm, respectively. The E and σ_1 plotted as a function of fibre diameter fitted the power functions with $R^2 > 0.93$.

To prove that the obtained results were an intrinsic property of the fibres and not a systematic error, AFM working in force spectroscopy mode was used. In these measurements, similar trend was found (Fig. 3d). E_{JKR} was 388 ± 22, 301 ± 18 and 160 ± 15 MPa for fibres 0.25 mm, 0.41 mm and 1.07 mm, respectively.

3.3. Crystallinity and molecular structure of fibres

DSC, WAXS and FTIR measurements were conducted to analyse the degree of crystallinity, X_c. X_c values obtained by DSC (Fig. 4) oscillated around 51% with very slight declining trend towards thicker fibres. To exclude the effect of possible variations in heat transfer caused by differences in contact areas between sample and the pan, which could lead to calculation of erroneous X_c [45] during DSC analysis, the WAXS was conducted (Fig. 5). We found strong declining trend of X_c by WAXS in a

function of increasing fibre diameter. The crystallinity decreased by over 10% from 59.2% for 0.18 mm fibres, through 52.2% for 0.41 mm fibres, to 48.5% for 1.07 mm fibres. From FTIR analysis of the C=O stretching vibration region (Fig. 6a and b), which is widely used to investigate the structure and degradation of biomaterials [46–48], we assessed that the X_c calculated as a Ac/(Ac + Aa), where Ac = A3, was slightly higher for thinner fibres. When Ac = A1 + A2 + A3, the value of X_c was higher, however, the declining trend was weaker (Fig. 6c).

DSC, WAXS and FTIR signals allowed us to analyse additional aspect of molecular structure of fibres. For example, the DSC data revealed that the shape of melting endotherm varied between different types of fibres. The peak minimum of T_m (1st heating), presented in Fig. 4a, was in the range from 62.2 °C to 63.9 °C; moreover, the trend that fibres with larger diameter had higher T_m occurred. Besides that, the start point of the transition was almost the same for all types of fibres, with the difference that the thinner fibres had sharper peaks and transition thereof finished at lower temperatures. The shape of the DSC curves obtained from thinner fibres suggests smaller crystals size, wide range of their distribution and/or weaker arrangement of them in comparison to thicker fibres.

Radial profile of WAXS analysis indicated three peaks for (110), (111) and (200) planes characteristic for orthorhombic PCL crystal lattices [49]. We observed that with the increase of the diameter of fibres, slight shift to lower 2Θ values of the mentioned peaks occurred (Fig. 5a). Moreover, the increase of values of FWHM of peaks for (111) and (200) planes was observed, whereas it decreased for plane (110).
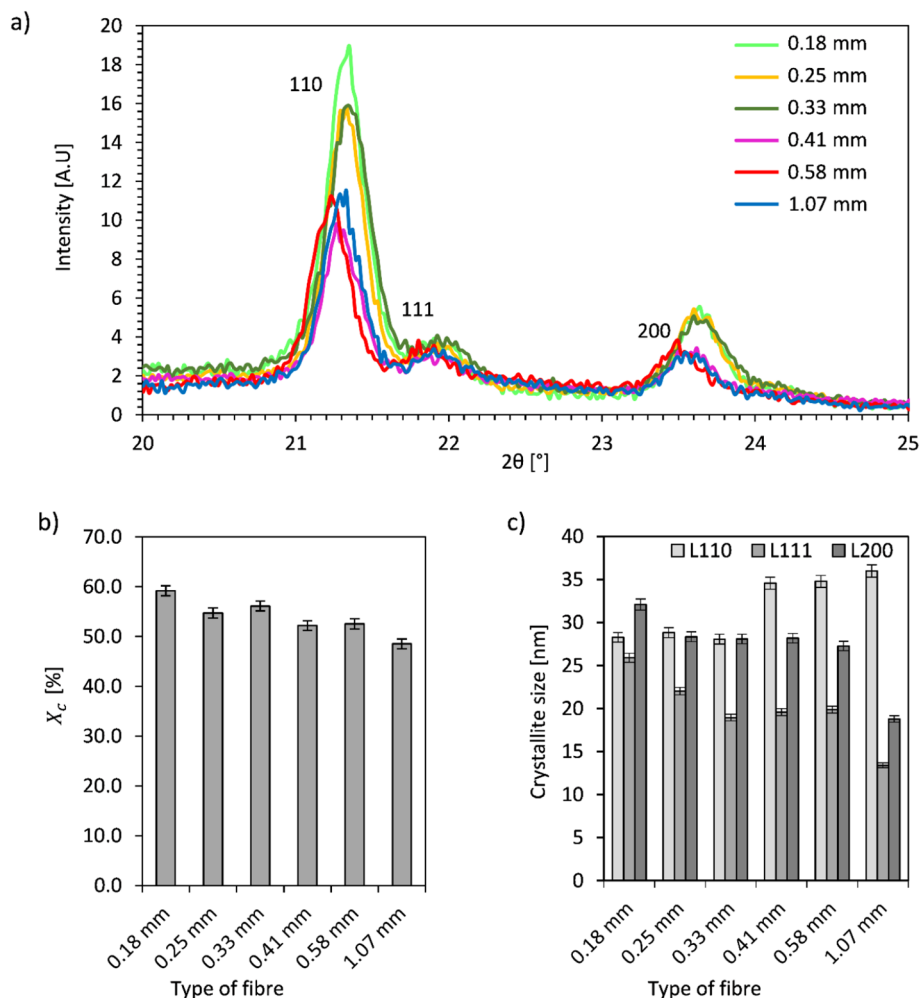

Fig. 5. a) WAXS radial profile of PCL samples in the range of 2Θ from 20° to 25° presenting the shift of peaks, b) degree of crystallinity X_c calculated from WAXS, c) crystallite size in (110), (111) and (200) planes in PCL crystal lattices.
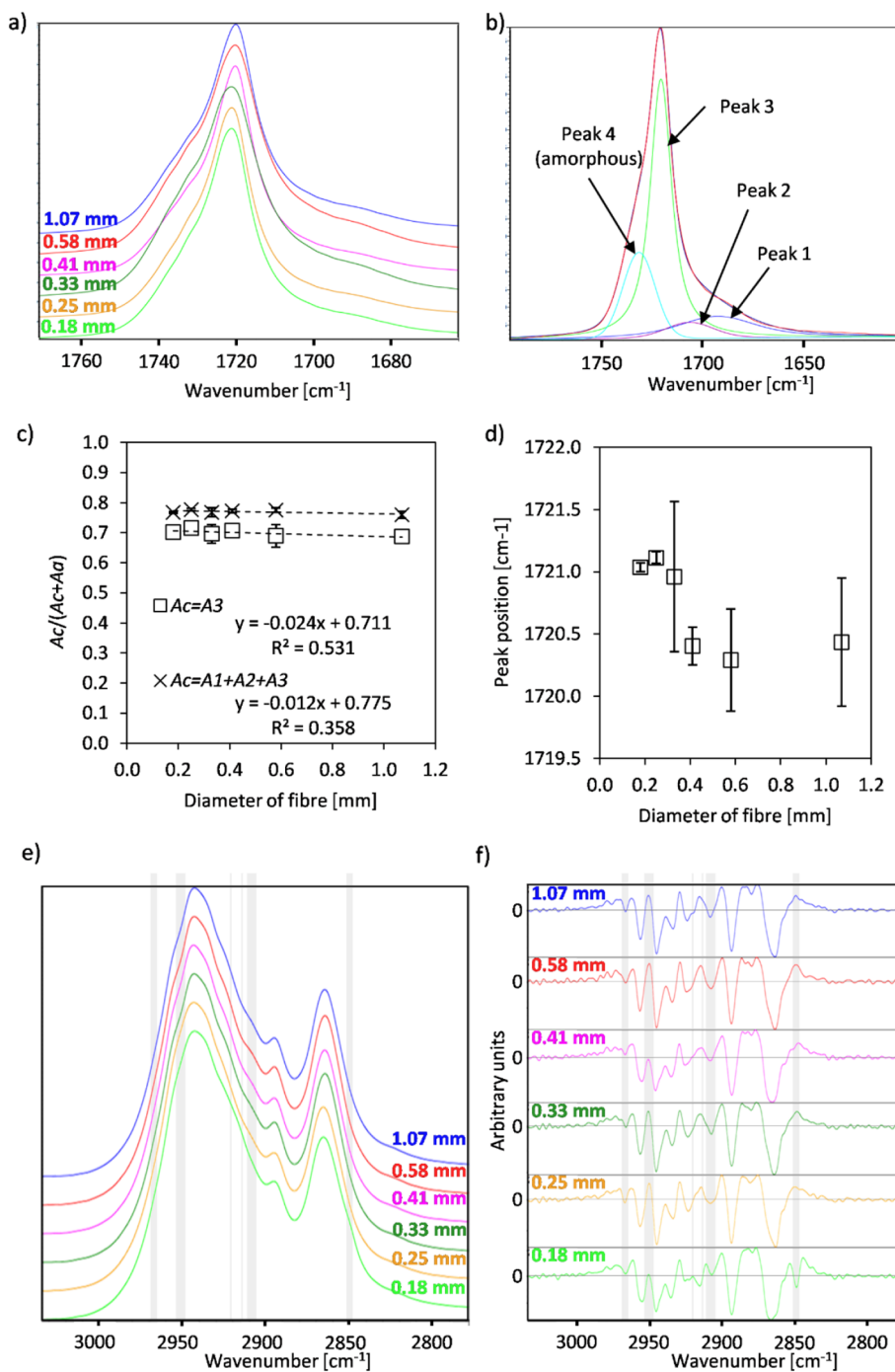
Fig. 6. a) The IR spectra in the C═O stretching vibration region, b) carbonyl band peak resolved into four components of Voight's peaks, c) degree of crystallinity X_c calculated as a ratio of Ac/(Ac + Aa), where Ac was the area of peak(s) derived from crystalline band (with or without peaks "1" and "2" derived from C═O with CH$_2$ interactions) and Aa was the area of peak derived from amorphous band, d) plot of maximum position of peak 3 as a function of fibre dimeter, e) the obtained spectra of PCL in the CH$_2$ stretching vibration region and f) 2nd derivatives thereof with shadowed areas depicting the regions where changes in frequency occurred.

From Scherrer's equation it is known that FWHM is directly linked with crystallite dimensions along the direction perpendicular to the crystallographic plane (*hkl*). Determined crystallites sizes in the aforementioned directions are presented in Fig. 5c. Decrease of crystallite dimensions along normal to (111) and (200) planes for thicker fibres was observed. In the case of 110 plane, increase of crystallite size was recorded. Additionally, there is more than two folds difference between the dimension of crystallites L200 and L110 or L111 for 1.07 mm fibres, whereas for 0.18 mm fibres all dimensions of crystallites were very similar.

FTIR spectroscopy is a highly sensitive tool to detect structural changes occurring during crystallisation [50]. In this study, the FTIR analysis showed change of the position of carbonyl peak derived from crystalline phase (Fig. 6d). For thicker fibres, the maximum of the peak was shifted to lower values of wavenumber. Moreover, in region of asymmetric stretching modes of CH$_2$ group of crystalline PCL, more peaks (apparent as more inflections of signal or zero value in 2nd derivative) originating from presence of hydrogen bonds [43,44] were observed for thicker fibres (Figs. 6e and f).

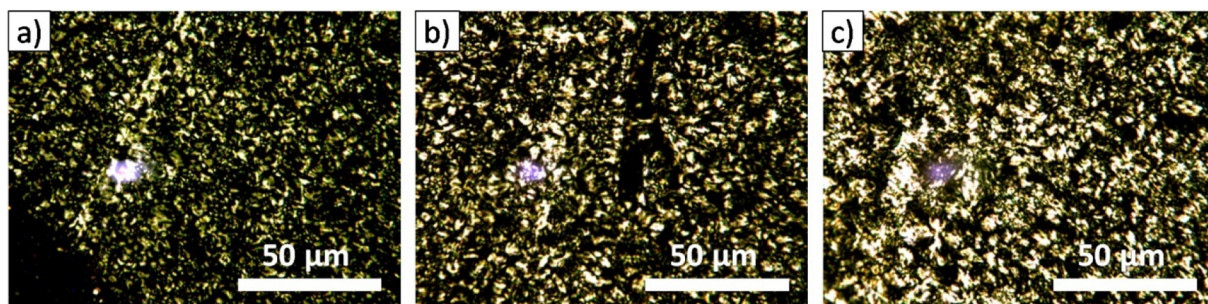Spherulites present in semi-crystalline polymers consist of lamellas

Fig. 7. PLM microphotographs of ultra-thin slices obtained from cross-sections of 0.25 mm (a), 0.41 mm (b) and 1.07 mm (c) fibres.

built from crystals and amorphous phase distributed between them. In case of the investigated fibres, the spherulites size increased with fibre diameter (Fig. 7). Qualitative analysis of the micrographs clearly shows that the spherulites present in the 0.25 fibres were much smaller than those in the 1.07 mm fibres.

4. Discussion

In this study, the relation between the diameter of micro-extruded PCL fibres and their mechanical properties was investigated. The obtained results showed that thinner fibres had higher Young's modulus and yield strength. This corresponded to changes in crystallinity and crystalline structure of the obtained fibres.

It is known, that the mechanical properties of materials depend on their microstructure. In the case of semi-crystalline polymers, their chains can form amorphous and crystalline phases, which are soft and hard, respectively. Since the crystalline phase is denser and acts as a reinforcement of the amorphous one, their ratio influences various material properties, including the stiffness [27,28]. Therefore, the first step towards explanation of the relation between the diameter of fibres and mechanical properties thereof was the measurement of the crystallinity. To exclude the possibility of systematic measurement error, we decided to employ three techniques used for determination of this parameter. DSC and FTIR analysis showed no clear decreasing trend between crystallinity and the fibre diameter, whereas WAXS results show distinctly lower values of X_c for thicker fibres. The difference between values of X_c obtained using these three analytical methods was caused by different phenomena being measured and their different sensitivity to presence of crystal defects and variations in microstructure [44,51–53]. Thus, complex analysis of the results produced by aforementioned methods was performed and a large variety within microstructure of the fibres was detected.

During fabrication process, the material was heated to 100 °C and the surrounding temperature was constant for all samples. However, heat transfer during cooling was not the same. It was observed that thinner fibres cooled down much faster than thicker one (Fig. 1b). This was related to the mass of extruded material per unit of length, which was higher for thicker fibres. It is commonly known that when the difference between ambient and material temperatures is the same, the heat transfer strongly depends on the mass of the sample. We estimate that the ratio of mass per unit of length of 1.07 mm and 0.18 mm fibres was approximately 35; therefore, the cooling rate for fibres 0.18 mm was much higher than for 1.07 mm. Since the crystallisation temperature (T_c) decreases with increasing cooling rate, the non-isothermal crystallisation of the fibre melt was accelerated in the case of smaller fibres [54]. The effect of cooling rate on spherulite morphology was clearly visible on PLM images (Fig. 7), where the slowly cooled big-diameter fibres had the biggest spherulites. This is consistent with the reported studies investigating the effect of cooling rate on spherulite size [55,56] In the case of thinner fibres, when faster cooling occurred, larger number of nucleation centres appeared in the initial state of crystallisation and it limited spherulites growth. As the result, small-diameter fibres had higher number of, however, smaller spherulites.

Another possible parameter affecting spherulite morphology is the shear stress during extrusion of the molten material. Janeschitz-Kriegl and co-workers demonstrated strong influence of shear rate applied in a range 20–150 s^{-1} on microstructure [57]. The authors demonstrated formation of higher number of nucleation centres at higher shear rates which yielded smaller spherulites. Moreover, different nozzle diameters could affect the temperatures of material inside of the nozzle and additionally change the nucleation rate.

Drawing of fibres, which is related to the movement of printing head in XY plane and flow rate of polymer melt, can cause the stress induced crystallisation, thus, affect microstructure of the fabricated fibres [58]. In this study, to obtain smooth surface and desired diameter of the fibres, the F was adjusted for each type of fibres in the range between 20 and 95 mm/min (see Table 1). The aforementioned feed rates were below those determined by McIlroy and Graham that alter crystallisation [58]. Moreover, we did not observe any correlation between the applied feed rates and neither of the measured microstructural parameters, e.g. spherulites morphology, nor mechanical properties.

All aforementioned phenomena could cause differences in arrangement at the macromolecular level which was demonstrated by in-depth DSC, WAXS and FTIR analyses. The direct effect of the different cooling rates on T_c, and thus on the microstructure and perfection of crystalline regions, could be observed as a change in T_m and in sharpness of peak of fusion measured in the 1st heating run of DSC [54,59]. In this study, sharpness and shift of peak minimum of the melting endotherms (T_m) towards lower temperatures was observed for fibres with smaller diameters (Fig. 4), suggesting existence of smaller or less arranged crystalline regions. This was also proved in WAXS. The results showed more than two folds difference between the dimension of crystallites in (110) and (200) or (111) directions for 1.07 mm fibres, whereas all dimensions were very similar for 0.18 mm fibres (Fig. 5c).

In FTIR analysis, alterations in carbonyl and methylene bands might be caused by change of electronegativity of neighbouring atoms due to formation of C–H···O=C interactions. It was shown for the blends of PCL with hydrogen-bonding donor polymers that the additional strong peaks in carbonyl band appeared [43,60] and were shifted towards lower wavelength after increasing the concentration of the donor polymer [60]. In a recent study, Funaki and co-workers underlined the existence of three types of C–H···O=C interactions (two inter- and one intramolecular) in pristine PCL. [44] The authors presented its impact on position of C=O band derived from crystalline phase and appearance of additional peaks in region of asymmetric stretching modes of CH$_2$ of crystalline PCL. In another recent study, Sangroniz and co-workers underlined the striking differences in, e.g., viscosity or crystallisation of self-nucleated and isotropic melts of PCL due to various probabilities of formation of hydrogen bonds [61]. In the present study, the difference in C–H···O=C interactions were visible as the shift of peak 3 deconvoluted from carbonyl band, and considered to originate from crystalline phase (Fig. 6d). Additionally, we observed in crystalline phase of PCL changes in the appearance of some peaks or in their

intensity in the region of asymmetric stretching (Fig. 6e) and deformation (Fig. A1 in Supplementary Data) modes of CH_2. More or stronger peak, which originated plausibly from higher input of hydrogen bonds, were recorded for larger fibres. This can be explained by lower cooling rate and smaller arrangement of polymer chains inside the nozzle in *meso* state which could enhance intermolecular dipole-dipole interactions (like hydrogen bonds) and cause increase of their fraction. Similarly, increase of dipole-dipole fraction after heating PCL, up to the melting point, was observed in recent work by Kotula and co-workers using Raman spectroscopy [62].

Using WAXS analysis, we showed that the lower cooling rate of thicker fibres played an important role in growth of the crystalline regions [63]. The relation was especially clear in the direction perpendicular to (110) plane of the crystalline lattice, where the shortest possible $C-H\cdots O=C$ interactions can be created [44]. Moreover, increased fraction of hydrogen bonds induced the expansion of crystal lattice in thicker fibres, as it was reported in other biodegradable polymers, namely, poly(glycolic acid) or poly(hydroxybutyrate) [44,52]. In this study, the shift of peaks to lower 2Θ value (Fig. 5a) which, according to Braggs's law, corresponds to an increase in distance between lattice planes and the expansion of crystal lattice was observed for thicker fibres.

Furthermore, the effects of hydrogen bonds may significantly influence the interpretation of relation between X_c and mechanical properties. Sato et al. [52] estimated that the energy of the $C-H\cdots O=C$ bond in poly(hydroxybutyrate) contributed to less than one third of the measured heat of fusion and could lead to significant overestimation of the calculated crystallinity in DSC. Alternatively, the enthalpy of pure crystals of PCL deformed by presence of H-bonds might be lower than reported in the literature, giving rise to possibly erroneous value of crystallinity measured by DSC [43]. Similarly, the FTIR analysis revealed no clear declining trend of changes in X_c in function of fibre diameter; moreover, considering the Ac as the (A3 + A2 + A1), the slight declining trend became more imperceptible. The reason may be that in the methods of calculation of X_c by DSC and FTIR analysis, the difference in signals given by fraction of hydrogen bonds overlaps with the measured signals. Nevertheless, in the thicker fibres, more $C-H\cdots O=C$ interactions or types of interactions were present, which was visible in the CH_2 regions of the FTIR spectrum. On the other hand, the over 90% correlation between mechanical properties of the investigated fibres and the X_c measured by means of WAXS (Table A2 in Supplementary Data) could be explained by the sensitivity of this method to presence of the defects in crystalline region, e.g. expansion of crystal lattice due to presence of H-bonds [43,44] or by the inhibition of growth of crystalline region due to bigger fraction of H-bonds formed [43] upon slower cooling of thicker fibres after extrusion.

In Fig. 8 we schematically presented the variations in microstructures and mechanical properties of PCL fibres in the tested range of diameters. With increase of diameter of fibre larger spherulites were observed, however lower content of crystalline phase with elongated crystallites and expanded crystal lattice occurred. The abovementioned variations can be explained by differences in molecular orientation inside the nozzle and cooling rate during extrusion. The second factor affected the durability of molecular order obtained in the nozzle due to shear and had strong impact on crystallisation after extrusion. It seems that the higher shear rate and temperature gradient inside the thinner nozzle decreased the possibility of creation of supramolecular interactions in PCL, like H-bonds. Whereas in thicker fibres weaker molecular order occurred and more hydrogen bonds were formed in meso state, affecting the size and shape of obtained crystalline lattice and crystallites, thus also mechanical properties of the polymer. Reported finding are consistent with results of terahertz spectroscopy performed by Funaki et al., showing that the intermolecular interactions in PCL are built first during the formation of lamella [44]. Thus, during slow crystallisation and at higher entropy of the system when crystallisation begun, the formation of larger fraction of H-bonds was more plausible.

Moreover, the formed hydrogen bonds inhibited the progression of crystallisation of thicker fibres after extrusion. That was proved in additional experiment, the analysis of the changes of degree of crystallinity in time measured by DSC (see Fig. A2 in Supplementary Data).

We also investigated the effect of lower cooling rate on the mechanical properties of the 0.18 mm and 0.25 mm fibres by printing them at ambient and increased temperature of platform. Deposition on the warm platform (45 °C) was aimed to induce lower cooling rates. It decreased the stiffness of both types of fibres by 15–20%, when compared with the stiffness of fibres deposited at ambient temperature (Fig. A3b in Supplementary Data). Moreover, reduction of the cooling rate cancelled the correlation between fibre diameter and stiffness; values of E measured for both types of fibres printed on the warm platform were similar ($p > 0.5$). Additionally, a shift of T_m towards higher temperatures and no changes in H_m was observed. The former suggests increase of size and/or molecular arrangement of the crystals. On the other hand, the lack of changes in the H_m combined with simultaneous decrease in E is yet another example of the contribution of hydrogen bonds to the enthalpy of fusion measured by DSC. Those observations support our findings regarding the relationship between the cooling rate, formation of the hydrogen bonds and the stiffness of the investigated fibres.

The aforementioned supramolecular interactions measured for the fibres made of PCL 70–90 kDa affected mechanical properties thereof. In additional experiment, we wanted to investigate whether the supramolecular interactions, and thus the mechanical properties, could be affected by the molecular weight of the PCL. To this end, we performed tensile tests and DSC measurements using fibres made of PCL with lower MW (M_n 45 kDa, Sigma-Aldrich). We observed similar fibre diameter-dependent trends for tensile modulus and thermal properties as those obtained for M_n PCL 70–90 kDa (Fig. A4 in Supplementary Data), i.e. the modulus decreased and T_m was shifted towards higher temperatures with increasing diameter of the fibres.

Another concern worth investigating is that during additive manufacturing of 3D scaffolds, the fibres are stacked upon each other. The deposition of melt of polymer on already deposited and solidified fibres might change their microstructure, thus mechanical properties. To address this issue, we performed annealing of two types of fibres, printed with nozzles with ID 0.25 mm and 1.07 mm, at 50 °C for 24 h. The annealing temperature was chosen based on infrared imaging taken during fabrication. The effect of annealing on thermal properties and stiffness is presented in Fig. A3c-d in Supplementary Data. Although we recorded change of shape of the melting endotherm and a shift of the melting point, the measured changes in stiffness were not significant. Therefore, we believe that the stiffness of material in stacking points of 3D porous scaffolds will be strongly linked to stiffness of extruded fibre and should not be significantly affected by micro-annealing caused by heat of deposited fibre from upper layer. Nevertheless, in FDM-printed porous scaffolds, there are other architectural parameters that determine its mechanical properties significantly, i.e. pattern, layer thickness or distance between fibres in single layer, due to its impact on porosity and contact area between layers. Moreover, other processing parameters, e.g. the temperature of extruded material strongly influence the stacking by changing the capacity of diffusion or re-entangling of polymer chains at interface between layers [64]. All mentioned parameters can be used to adjust the macroscopic mechanical properties of scaffolds. However, the difference in nanoscale properties due to variations in microstructure can be modulated only by previously analysed phenomena in this study. It is important to consider the difference in microstructure of fibres, thus the properties, as in most of the TE applications, scaffolds should exhibit high porosity, which imposes increased distance between fibres. In scaffolds with high porosities, i.e. > 50%, the fraction of fibres which are not in contact with each other is higher than the fraction of fibres which are stacked upon each other. Therefore, the unbounded segments of fibres and its microstructure play important role in TE scaffolds.
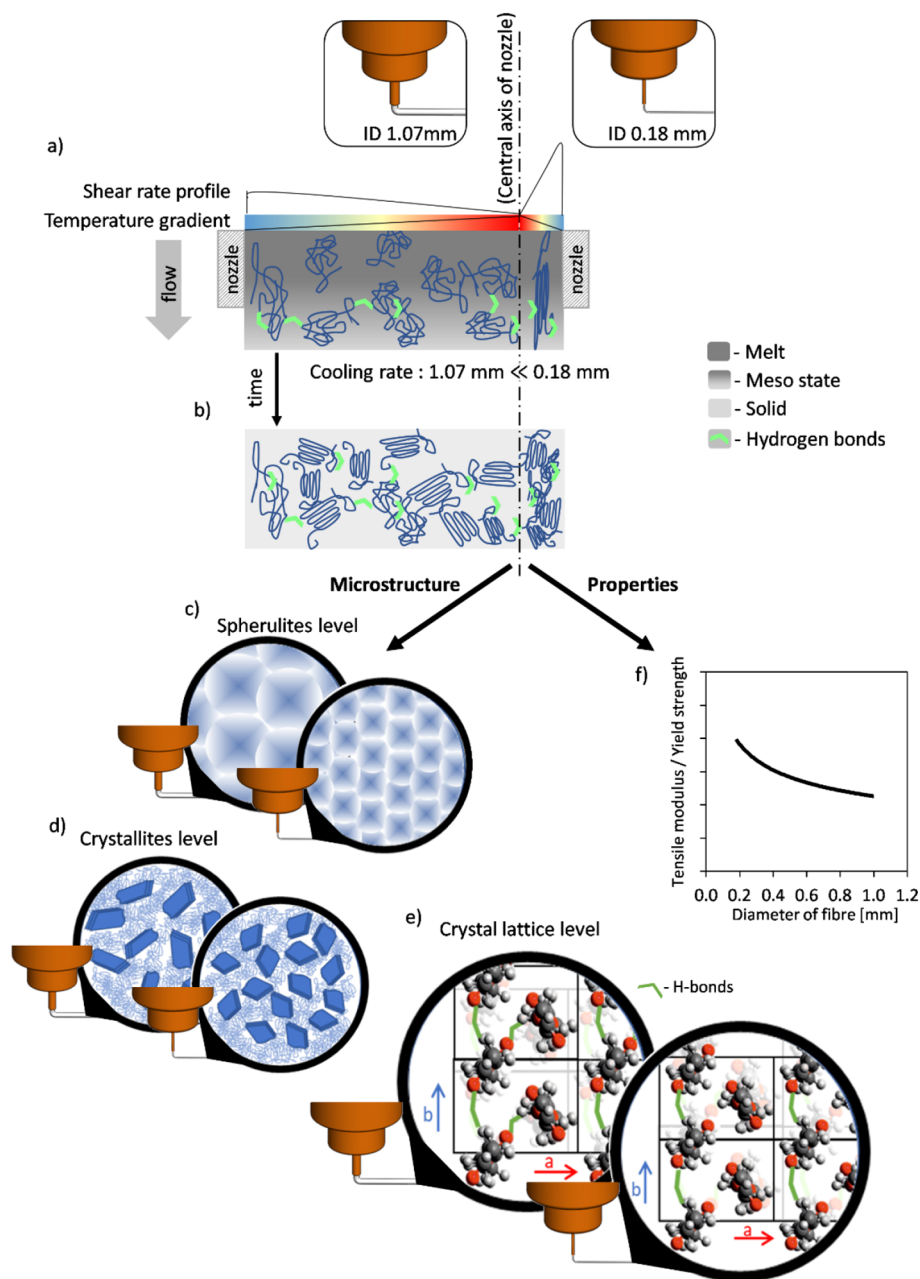
Fig. 8. The schematic presentation of changes in microstructures and mechanical properties of PCL fibres fabricated by extrusion through nozzles in range of ID 0.18 mm – 1.07 mm: a) the effect of shear rate and temperature gradient inside the nozzle on molecular orientation; in ID 1.07 mm weaker order and more hydrogen bonds were formed due to lower shear rate and slower cooling; b) lower cooling rate of thicker fibres and corresponding higher temperature of crystallisation induced formation of bigger fraction of hydrogen bonds, which inhibited the crystallisation after extrusion; c) changes in microstructure at spherulites level: bigger spherulites formed in thicker fibres due to the lower cooling and shear rates; d) changes in microstructure at crystallite level: smaller fraction of crystalline phase but crystallites are more elongated than in thinner fibres; e) changes in microstructure at crystal lattice level: presence of bigger fraction/more types of hydrogen bonds in thicker fibres caused the expansion of crystal lattice comparing to thinner fibres; f) the tensile modulus and yield strength in a function of fibre diameter are the macroscopic manifestation of the variations in microstructure arose from fabrication process.

5. Conclusions

The converse correlation between the mechanical properties and the diameter of 3D-printed fibres made of PCL was found. The relation strongly depended on the microstructure induced by the fabrication process, thus spontaneous cooling rate and shear occurring in the nozzle. The obtained results demonstrated the differences present at each analysed level of microstructure. With increase of diameter of fibre larger spherulites were observed, however lower content of crystalline phase with elongated crystallites and expanded crystal lattice occurred. The observed differences between fibres were related with formation of hydrogen bonds which varied during processing and affected the crystallisation of polymeric chains.

Taken together, the results obtained in the present study shed light on the phenomena occurring during the fabrication of PCL fibres by the FDM method. Moreover, they reveal the complexity of process – microstructure – property dependence and how they can be affected during fabrication. In conclusion, the present study demonstrates that the diameter of the PCL fibres should be considered as a parameter which may affect the mechanical properties of 3D-printedscaffolds due to changes of the microstructure of polymer during extrusion process.

CRediT authorship contribution statement

Żaneta Górecka: Conceptualization, Investigation, Writing - original draft, Writing - review & editing.**Joanna Idaszek:** Conceptualization, Investigation, Writing - original draft, Writing - review & editing.**Dorota Kołbuk:**Investigation, Writing - review & editing.**Emilia Choińska:**Investigation, Writing - review & editing.**Adrian Chlanda:**Investigation, Writing - review & editing.**Wojciech Święszkowski:**Conceptualization, Writing - review & editing.

Declaration of competing interest

The authors declare that they have no known competing financial

interests or personal relationships that could have appeared to influence the work reported in this paper.

Acknowledgments

Appendix A. Supplementary data

Supplementary data to this article can be found online at https://doi.org/10.1016/j.msec.2020.111072.

References

[1] J. Idaszek, E. Kijeńska, M. Łojkowski, W. Swieszkowski, How important are scaffolds and their surface properties in regenerative medicine, Appl. Surf. Sci. 388 (2016) 762–774.

[2] I. Zein, D.W. Hutmacher, K.C. Tan, S.H. Teoh, Fused deposition modeling of novel scaffold architectures for tissue engineering applications, Biomaterials 23 (2002) 1169–1185.

[3] S. Giannitelli, D. Accoto, M. Trombetta, A. Rainer, Current trends in the design of scaffolds for computer-aided tissue engineering, Acta Biomater. 10 (2014) 580–594.

[4] D.W. Hutmacher, T. Schantz, I. Zein, K.W. Ng, S.H. Teoh, K.C. Tan, Mechanical properties and cell cultural response of polycaprolactone scaffolds designed and fabricated via fused deposition modeling, J. Biomed. Mater. Res. A 55 (2001) 203–216.

[5] M. Vaezi, H. Seitz, S. Yang, A review on 3D micro-additive manufacturing technologies, Int. J. Adv. Manuf. Technol. 67 (2013) 1721–1754.

[6] J. Malda, T. Woodfield, F. Van Der Vloodt, C. Wilson, D. Martens, J. Tramper, C. Van Blitterswijk, J. Riesle, The effect of PEGT/PBT scaffold architecture on the composition of tissue engineered cartilage, Biomaterials 26 (2005) 63–72.

[7] T.B. Woodfield, J. Malda, J. De Wijn, F. Peters, J. Riesle, C.A. van Blitterswijk, Design of porous scaffolds for cartilage tissue engineering using a three-dimensional fiber-deposition technique, Biomaterials 25 (2004) 4149–4161.

[8] T. Woodfield, C.V. Blitterswijk, J.D. Wijn, T. Sims, A. Hollander, J. Riesle, Polymer scaffolds fabricated with pore-size gradients as a model for studying the zonal organization within tissue-engineered cartilage constructs, Tissue Eng. 11 (2005) 1297–1311.

[9] L. Moroni, J. De Wijn, C. Van Blitterswijk, Three-dimensional fiber-deposited PEOT/PBT copolymer scaffolds for tissue engineering: influence of porosity, molecular network mesh size, and swelling in aqueous media on dynamic mechanical properties, J. Biomed. Mater. Res. A 75 (2005) 957–965.

[10] L. Moroni, J. De Wijn, C. Van Blitterswijk, 3D fiber-deposited scaffolds for tissue engineering: influence of pores geometry and architecture on dynamic mechanical properties, Biomaterials 27 (2006) 974–985.

[11] L. Moroni, G. Poort, F. Van Keulen, J. De Wijn, C. Van Blitterswijk, Dynamic mechanical properties of 3D fiber-deposited PEOT/PBT scaffolds: an experimental and numerical analysis, J. Biomed. Mater. Res. A 78 (2006) 605–614.

[12] R. Landers, R. Mülhaupt, Desktop manufacturing of complex objects, prototypes and biomedical scaffolds by means of computer-assisted design combined with computer-guided 3D plotting of polymers and reactive oligomers, Macromol. Mater. Eng. 282 (2000) 17–21.

[13] R. Landers, A. Pfister, U. Hübner, H. John, R. Schmelzeisen, R. Mülhaupt, Fabrication of soft tissue engineering scaffolds by means of rapid prototyping techniques, J. Mater. Sci. 37 (2002) 3107–3116.

[14] R. Landers, U. Hübner, R. Schmelzeisen, R. Mülhaupt, Rapid prototyping of scaffolds derived from thermoreversible hydrogels and tailored for applications in tissue engineering, Biomaterials 23 (2002) 4437–4447.

[15] A. Pfister, R. Landers, A. Laib, U. Hübner, R. Schmelzeisen, R. Mülhaupt, Biofunctional rapid prototyping for tissue-engineering applications: 3D bioplotting versus 3D printing, J. Polym. Sci. A Polym. Chem. 42 (2004) 624–638.

[16] C. Carvalho, R. Landers, U. Hübner, R. Schmelzeisen, R. Mülhaupt, Fabrication of soft and hard biocompatible scaffolds using 3D-bioplotting, Virtual Modelling and Rapid Manufacturing-Advanced Research in Virtual and Rapid Prototyping, Taylor & Francis Group, London, England, 2005, pp. 97–102.

[17] D.W. Hutmacher, M. Sittinger, M.V. Risbud, Scaffold-based tissue engineering: rationale for computer-aided design and solid free-form fabrication systems, Trends Biotechnol. 22 (2004) 354–362.

[18] F. Wang, L. Shor, A. Darling, S. Khalil, W. Sun, S. Güçeri, A. Lau, Precision extruding deposition and characterization of cellular poly-ε-caprolactone tissue scaffolds, Rapid Prototyp. J. 10 (2004) 42–49.

[19] A. Di Luca, B. Ostrowska, I. Lorenzo-Moldero, A. Lepedda, W. Swieszkowski, C. Van Blitterswijk, L. Moroni, Gradients in pore size enhance the osteogenic differentiation of human mesenchymal stromal cells in three-dimensional scaffolds, Sci. Rep. 6 (2016) 22898.

[20] B. Ostrowska, A. Di Luca, L. Moroni, W. Swieszkowski, Influence of internal pore architecture on biological and mechanical properties of three-dimensional fiber

[21] Y. Rotbaum, C. Puiu, D. Rittel, M. Domingos, Quasi-static and dynamic in vitro mechanical response of 3D printed scaffolds with tailored pore size and architectures, Mater. Sci. Eng. C 96 (2019) 176–182.

[22] H. Tsuji, Y. Ikada, Blends of aliphatic polyesters. I. Physical properties and morphologies of solution-cast blends from poly (DL-lactide) and poly (ε-caprolactone), J. Appl. Polym. Sci. 60 (1996) 2367–2375.

[23] A. Larrañaga, E. Diamanti, E. Rubio, T. Palomares, A. Alonso-Varona, P. Aldazabal, F. Martin, J. Sarasua, A study of the mechanical properties and cytocompatibility of lactide and caprolactone based scaffolds filled with inorganic bioactive particles, Mater. Sci. Eng. C 42 (2014) 451–460.

[24] W. Hendrikson, J. Rouwkema, C. Van Blitterswijk, L. Moroni, Influence of PCL molecular weight on mesenchymal stromal cell differentiation, RSC Adv. 5 (2015) 54510–54516.

[25] C. Bastioli, A. Cerutti, I. Guanella, G. Romano, M. Tosin, Physical state and biodegradation behavior of starch-polycaprolactone systems, J. Polym. Environ. 3 (1995) 81–95.

[26] H. Chen, L. Li, T. Lin, Formation of segregation morphology in crystalline/amorphous polymer blends: molecular weight effect, Macromolecules 31 (1998) 2255–2264.

[27] C. Ng, S. Teoh, T. Chung, D. Hutmacher, Simultaneous biaxial drawing of poly (ε-caprolactone) films, Polymer 41 (2000) 5855–5864.

[28] G. Sekosan, N. Vasanthan, Morphological changes of annealed poly-ε-caprolactone by enzymatic degradation with lipase, J. Polym. Sci. B Polym. Phys. 48 (2010) 202–211.

[29] D. Kołbuk, P. Sajkiewicz, K. Maniura-Weber, G. Fortunato, Structure and morphology of electrospun polycaprolactone/gelatine nanofibres, Eur. Polym. J. 49 (2013) 2052–2061.

[30] La Mantia, F. P.; Ceraulo, M.; Mistretta, M. C.; Morreale, M. Effect of cold drawing on mechanical properties of biodegradable fibers. Journal of applied biomaterials & functional materials 2017, 15.

[31] J.M. Dealy, K.F. Wissbrun, Melt Rheology and Its Role in Plastics Processing: Theory and Applications, Springer Science & Business Media, 2012.

[32] F. Hou, D. Mi, M. Zhou, J. Zhang, The influences of a novel shear layer-spherulites layer alternated structure on the mechanical properties of injection-molded isotactic polypropylene, Polymer 122 (2017) 12–21.

[33] A. Di Luca, K. Szlazak, I. Lorenzo-Moldero, C.A. Ghebes, A. Lepedda, W. Swieszkowski, C. Van Blitterswijk, L. Moroni, Influencing chondrogenic differentiation of human mesenchymal stromal cells in scaffolds displaying a structural gradient in pore size, Acta Biomater. 36 (2016) 210–219.

[34] G. Pezzin, G. Gechele, Capillary viscometry of molten polycaprolactam, J. Appl. Polym. Sci. 8 (1964) 2195–2212.

[35] A. Chlanda, E. Kijeńska, W. Święszkowski, In in microscopic methods for characterization of selected surface properties of biodegradable, nanofibrous tissue engineering scaffolds, Materials Science Forum; Trans Tech Publ 890 (2017) 213–216.

[36] A. Chlanda, P. Oberbek, M. Heljak, Ż. Górecka, K. Czarnecka, K. Chen, M.J. Woźniak, Nanohydroxyapatite adhesion to low temperature plasma modified surface of 3D-printed bone tissue engineering scaffolds-qualitative and quantitative study, Surf. Coat. Technol. 375 (2019) 637–644.

[37] A. Chlanda, J. Rebis, E. Kijeńska, M.J. Wozniak, K. Rozniatowski, W. Swieszkowski, K.J. Kurzydlowski, Quantitative imaging of electrospun fibers by PeakForce Quantitative NanoMechanics atomic force microscopy using etched scanning probes, Micron 72 (2015) 1–7.

[38] Z. Gan, Q. Liang, J. Zhang, X. Jing, Enzymatic degradation of poly (ε-caprolactone) film in phosphate buffer solution containing lipases, Polym. Degrad. Stab. 56 (1997) 209–213.

[39] D. Kolbuk, S. Guimond-Lischer, P. Sajkiewicz, K. Maniura-Weber, G. Fortunato, The effect of selected electrospinning parameters on molecular structure of polycaprolactone nanofibers, Int. J. Polym. Mater. Polym. Biomater. 64 (2015) 365–377.

[40] M. Kakudo, N. Kasai, X-ray Diffraction by Polymers, (1972).

[41] Y. He, Y. Inoue, Novel FTIR method for determining the crystallinity of poly (ε-caprolactone), Polym. Int. 49 (2000) 623–626.

[42] S. Murphy, G. Leeke, M. Jenkins, A comparison of the use of FTIR spectroscopy with DSC in the characterisation of melting and crystallisation in polycaprolactone, J. Therm. Anal. Calorim. 107 (2012) 669–674.

[43] T. Honma, T. Senda, Y. Inoue, Thermal properties and crystallization behaviour of blends of poly (ε-caprolactone) with chitin and chitosan, Polym. Int. 52 (2003) 1839–1846.

[44] C. Funaki, S. Yamamoto, H. Hoshina, Y. Ozaki, H. Sato, Three different kinds of weak CH···O=C inter-and intramolecular interactions in poly (ε-caprolactone) studied by using terahertz spectroscopy, infrared spectroscopy and quantum chemical calculations, Polymer 137 (2018) 245–254.

[45] J. Crighton, F. Wilburn, The role of heat transfer in the production of DSC curves, Thermochim. Acta 203 (1992) 1–5.

[46] O. Urbanek, F. Pierini, E. Choińska, P. Sajkiewicz, M. Bil, W. Święszkowski, Effect of hydroxyapatite nanoparticles addition on structure properties of poly (L-lactide-co-glycolide) after gamma sterilization, Polym. Compos. 39 (2016) 1023–1031.

[47] E. Choinska, T. Muroya, W. Swieszkowski, T. Aoyagi, Influence of macromolecular structure of novel 2-and 4-armed polylactides on their physicochemical properties and in vitro degradation process, J. Polym. Res. 23 (2016) 1–11.

[48] D. Kolbuk, P. Sajkiewicz, P. Denis, E. Choinska, Investigations of polycaprolactone/gelatin blends in terms of their miscibility, Bulletin of the Polish Academy of Sciences: Technical Sciences 61 (2013) 629–632.

[49] H. Bittiger, R. Marchessault, W. Niegisch, Crystal structure of poly-ε-caprolactone, Acta Crystallographica Section B: Structural Crystallography and Crystal Chemistry 26 (1970) 1923–1927.

[50] S. Li, T. He, X. Liao, Q. Yang, G. Li, Structural changes and crystallization kinetics of polylactide under CO2 investigated using high-pressure Fourier transform infrared spectroscopy, Polym. Int. 64 (2015) 1762–1769.

[51] Z. Mo, H. Zhang, The degree of crystallinity in polymers by wide-angle x-ray diffraction (WAXD), J. Macromol. Sci. Polym. Rev. 35 (1995) 555–580.

[52] H. Sato, R. Murakami, I. Noda, Y. Ozaki, Infrared and Raman spectroscopy and quantum chemistry calculation studies of C–H···O hydrogen bondings and thermal behavior of biodegradable polyhydroxyalkanoate, J. Mol. Struct. 744 (2005) 35–46.

[53] P. Sajkiewicz, M. Heljak, A. Gradys, E. Choińska, S. Rumiński, T. Jaroszewicz, I. Bissenik, W. Święszkowski, Degradation and related changes in supermolecular structure of poly (caprolactone) in vivo conditions, Polym. Degrad. Stab. 157 (2018) 70–79.

[54] A. Wurm, E. Zhuravlev, K. Eckstein, D. Jehnichen, D. Pospiech, R. Androsch, B. Wunderlich, C. Schick, Crystallization and homogeneous nucleation kinetics of poly (ε-caprolactone) (PCL) with different molar masses, Macromolecules 45 (2012) 3816–3828.

[55] C. Zhang, L. Lu, W. Li, L. Li, C. Zhou, Effects of crystallization temperature and spherulite size on cracking behavior of semi-crystalline polymers, Polym. Bull. 73 (2016) 2961–2972.

[56] W. Dietz, Effect of cooling on crystallization and microstructure of polypropylene, Polym. Eng. Sci. 56 (2016) 1291–1302.

[57] H. Janeschitz-Kriegl, E. Ratajski, M. Stadlbauer, Flow as an effective promotor of nucleation in polymer melts: a quantitative evaluation, Rheol. Acta 42 (2003) 355–364.

[58] C. McIlroy, R. Graham, Modelling flow-enhanced crystallisation during fused filament fabrication of semi-crystalline polymer melts, Additive Manufacturing 24 (2018) 323–340.

[59] J. Zhang, K. Tashiro, H. Tsuji, A.J. Domb, Disorder-to-order phase transition and multiple melting behavior of poly (L-lactide) investigated by simultaneous measurements of WAXD and DSC, Macromolecules 41 (2008) 1352–1357.

[60] S.W. Kuo, C.F. Huang, F.C. Chang, Study of hydrogen-bonding strength in poly (ε-caprolactone) blends by DSC and FTIR, J. Polym. Sci. B Polym. Phys. 39 (2001) 1348–1359.

[61] L. Sangroniz, R. Alamo, D. Cavallo, A. Santamaría, A. Müller, A. Alegría, Differences between isotropic and self-nucleated PCL melts detected by dielectric experiments, Macromolecules 51 (2018) 3663–3671.

[62] A.P. Kotula, C.R. Snyder, K.B. Migler, Determining conformational order and crystallinity in polycaprolactone via Raman spectroscopy, Polymer 117 (2017) 1–10.

[63] G. Li, Self-healing Composites: Shape Memory Polymer Based Structures, John Wiley & Sons, 2014, pp. 179–180.

[64] V. Srinivas, C.S. van Hooy-Corstjens, G.B. Vaughan, B. van Leeuwen, S. Rastogi, J.A. Harings, Interfacial stereocomplexation to strengthen fused deposition modeled poly (lactide) welds, ACS Applied Polymer Materials (8) (2019) 2131–2139.